buildings

Article

# Seismic Bearing Capacity of Strip Foundation on Rock Mass Obeying Modified Hoek-Brown Failure Criterion

**Dianchun Du [1,2] and Zhentao Liu [1,2,*]**

[1] Key Laboratory of Concrete and Prestressed Concrete Structures of Ministry of Education, Southeast University, Nanjing 211189, China
[2] School of Civil Engineering, Southeast University, Nanjing 211189, China
* Correspondence: 230228296@seu.edu.cn

**Abstract:** The kinematic method of limit analysis theory was adopted in this paper to calculate the seismic bearing capacity of the shallow strip foundation on a rock mass obeying the non-linear modified Hoek-Brown failure criterion. The generalized Prandtl failure mechanism was chosen, which is different from the multi-wedge failure mechanism assumption commonly used in previous research. Three angle parameters were used to control the mechanism shapes, and the equivalent friction angle and equivalent cohesive were adopted to faithfully reflect the shape characteristics of the failure mechanism. The seismic action was considered using the pseudo-static method, which is simplified to the inertial force determined by the horizontal seismic coefficient. The validation of the present method was carried out by comparing with previous analytical results and the finite element model. Subsequently, the influences of the surface overload, the properties of the rock mass, and the seismic action on the shape and ultimate bearing capacity of the failure mechanism were investigated. For the convenience of practical engineering, this paper gives the ultimate bearing capacity of strip foundations on five representative rock foundations, and the variation trend of bearing capacity with the unit weight of rock mass, surface overload, and horizontal seismic coefficient.

**Keywords:** rocky foundation; seismic bearing capacity; modified Hoek-Brown criterion; limit analysis; generalized Prandtl mechanism



**Citation:** Du, D.; Liu, Z. Seismic Bearing Capacity of Strip Foundation on Rock Mass Obeying Modified Hoek-Brown Failure Criterion. *Buildings* **2022**, *12*, 2083. https://doi.org/10.3390/buildings12122083

Academic Editor: Marco Di Ludovico

Received: 7 November 2022
Accepted: 24 November 2022
Published: 28 November 2022



## 1. Introduction

Nowadays, more land resources are being converted to accommodate urban construction, including rocky foundations that were once difficult to develop upon [1–8]. Numerous residential buildings, office buildings, and transportation facilities that create large loads have been built on rocky foundations, and these facilities may be damaged or even destroyed during an earthquake, resulting in large economic and human losses. To ensure the safety of these facilities, engineers have focused their attention on the study of seismic bearing capacity of foundations [1]. The problem of concern in this study was the ultimate bearing capacity of strip foundations under the action of seismic load.

The methods used for shallow foundation bearing capacity assessment can be roughly divided into the following four categories: (1) the limit equilibrium method, (2) the slip-line method, (3) the limit analysis method, and (4) the numerical analysis method, based on finite element technique or finite difference technique [2–8]. The first three methods are all traditional soil mechanics analysis methods: the limit equilibrium method establishes a simplified failure mode that makes it possible to use simple statics methods to solve various problems. The slip-line method is used to derive the basic differential equation and then obtain the solutions of various problems by determining the slip-line network. Unlike the traditional limit equilibrium and slip-line methods, the limit analysis method selects a certain flow law to consider the stress-strain relationship of the soil in an idealized way. As for the numerical analysis methods, they are modern calculation means that are rapidly emerging following the development of computers. During the calculation process, the entire problem area is decomposed, and each sub-area becomes a simple part. For each unit, a suitable (simpler) approximate solution is assumed, and then the total satisfying conditions of this domain (such as structural equilibrium conditions) can be inferred to obtain the solution of the problem. The kinematics method selected for this study belongs to the limit analysis upper method, in which both the failure mechanism and energy consumption are considered. The upper limit of the actual failure load is obtained by simply selecting the appropriate stress field and velocity field, according to the principle that the external power must be equal to the internal power consumed by the mechanism. Since the foundation bearing capacity studied in this paper is an actual engineering problem, the safety conditions require that the bearing capacity should be greater than the maximum value of the calculated ultimate load, which means the foundation bearing capacity should be at the upper limit of the ultimate load.

The calculation of the ultimate bearing capacity of a foundation placed on a rock mass is a classic subject in the field of civil engineering [2,9–11]. Most analytical work is based on the general assumption that the strength of rock is dominated by the Mohr-Coulomb (MC) criterion as soil [12], under which the classical textbook of Terzaghi describes the bearing capacity of strip loads as [13]:

$$q_u = cN_c + q_0' N_q + \frac{1}{2}\gamma B_0 N_\gamma \tag{1}$$

where $c$ denotes soil cohesion; $q_0'$ is equivalent uniform load; $\gamma$ is unit weight of soil or rock mass; $B_0$ is foundation width; and $N_c,\ N_q,\ N_\gamma$ are the coefficients of Terzaghi bearing capacity, which are only determined by the friction angle $\varphi$.

The stress-strain relationship of most rock masses is nonlinear; this has been confirmed by numerous experiments [14–16]. Among the nonlinear failure criteria proposed in numerous studies, the Hoek-Brown (HB) criterion shows a preferable ability to simulate the strength properties of isotropic rock masses. Hoek et al. [17–20] proposed a method that can transform the various parameters ($m,\ s,\ n,\ GSI$, etc.) describing the properties of rock into the commonly used parameters $c$ and $\varphi$ of the MC criterion describing the properties of soil. After the transformation, the stress-strain relationship of the rock can be approximated by the MC criterion, and then the bearing capacity of the strip foundation placed on the rock mass can be calculated by the above-mentioned formula for the bearing capacity proposed by Terzaghi [13].

Based on the method used by Hoek et al. [17,19,21,22], Yang and Yin [12] assumed that the rock mass followed the modified HB criterion, while searching for the process of the bearing capacity for strip foundations on rock mass, and in which a certain optimal MC criterion tangent on the original HB curve is selected for substitution. This substitution transforms the stress-strain relationship of the foundation from the original nonlinear relationship described by the rock parameters ($m_i,\ s$, and $GSI$) into a linear relationship described by the soil parameters ($c$ and $\varphi$). Although this method has been adopted by some researchers, it overestimates the strength of the rock foundation, which leads to a subsequent overestimation of the ultimate bearing capacity of the foundation.

In addition, reductions in foundation bearing capacity caused by seismic motion is also a key concern in civil engineering. In many studies and engineering stability analyses, the effect of seismic motion on the foundation is usually modeled as a pseudo-static force, which has been shown to yield a relatively reliable estimate across a wide range of applications. Since the stability calculation is not considered in this paper, to simplify the calculation process, the seismic action is simplified to the load imposed on the structure by the proposed pseudo-static approach.

Most of the existing studies on the bearing capacity of rock foundations [12–14,23,24] have adopted the optimization method recommended by Drescher and Christopoulos [25] and Collins et al. [26]. The tangent angle (i.e., equivalent friction angle, $\varphi_t$) is determined by moving the position of the tangent point on the HB nonlinear damage envelope, and then the equivalent cohesion, $c_t$, is inferred from the equivalent friction angle, $\varphi_t$. The bearing capacity can be calculated according to the equivalent friction angle, $\varphi_t$, and cohesion, $c_t$. Finally, the process is repeated until the minimum value of the calculated bearing capacity is obtained.

However, due to the nonlinearity of the rock strength envelope, the slope of the tangent line varies greatly when the tangent point is located at different positions on the envelope, which explains why the slope of the equivalent MC strength line at the completion of the iteration does not correctly represent the trend of the nonlinear HB strength envelope. Referring to Hoek's summary based on extensive experimental and practical engineering experience [18,19], a method for calculating $c_t$ and $\varphi_t$ that can more realistically reflect the strength characteristics of the rock mass was chosen here. In the subsequent process, only the shape of the failure mechanism is changed without adjusting the values of $c_t$ and $\varphi_t$. This operation ensures that the selected $c_t$ and $\varphi_t$ are always representative of the bearing capacity characteristics of the rock mass.

One advantage of this method is that it can find the only optimal equivalent MC linear envelope that represents the trend of the HB nonlinear damage envelope. The results were compared with those of Yang and Yin [12], which verified the present work.

The present work was mostly focused on the evaluation of ultimate bearing capacity [12], and this paper extends this work to the calculation of the ultimate bearing capacity of a foundation under the influence of an earthquake. Additionally, this research further gives the five types of typical rock foundations on the strip foundation bearing capacity upper bounds and predictive failure mechanics. These failure mechanics can reflect the characteristics of each different rock mass. Lastly, the influences of surface overloading, the unit weight of a rock mass, the strength properties of a rock mass, and seismic action on foundation bearing capacity were studied. A set of seismic uniaxial compression bearing capacity coefficient tables summarizes the results of theoretical calculations. For practical application, the engineer can select the bearing capacity coefficients from the tables for different seismic intensities and multiply them by the uniaxial compressive strength, $\sigma_c$, of rock to get the upper limit of bearing capacity under different seismic intensities.

## 2. Problem Statement and Theoretical Framework

### 2.1. Geometric Description of the Structure and Basic Assumptions

The objective of this study was to seek the minimum value of the upper limit of the ultimate bearing capacity of a foundation expressed in the form of equivalent foundation load under the influence of an earthquake. This was assumed to be a plane strain problem with a homogeneous rock mass possessing infinite volume, and the failure mechanism was always inside the rock body. The problem was placed in the rectangular coordinate system $(e_1, e_2)$, as shown in Figure 1. A strip foundation of width $B_0$ was placed in a homogeneous rock mass of unit weight $\gamma$, and the bottom of the foundation was at a depth of $D$ from the horizontal ground surface. The solution of the bearing capacity, obtained under the condition that $D$ is much smaller than $B_0$, was called the shallow foundation solution, and the solution obtained when $D$ is much larger than $B_0$ was the deep foundation solution.

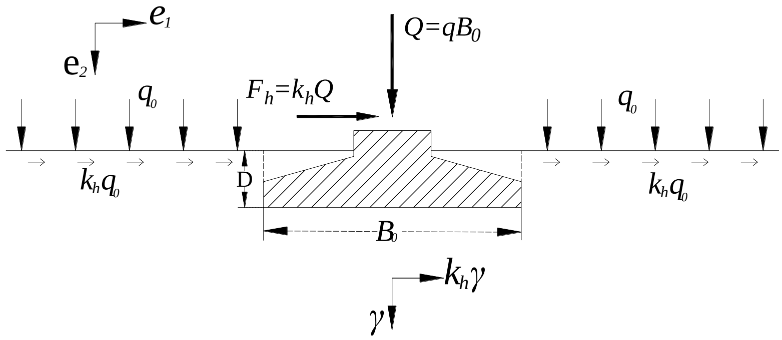


**Figure 1.** Strip foundation placed on rock mass.

The vertical load, $Q$, from the superstructure, the surface overload, $q_0$, and the horizontal seismic acceleration generated by the seismic wave passes are considered in the analysis. It should be noted that the significant changes in the magnitude and direction of the seismic acceleration in the rock mass are not considered in the analysis for the interests of simplicity. According to the research of Saada et al. [27], a concept of average seismic coefficient was adopted to calculate the acceleration distribution in rock mass, only considering the horizontal component of the seismic acceleration. The horizontal component was assumed to be homogeneous within the range of the rock mass involved in the failure mechanism.

The specific loading pattern is presented in Figure 1. The vertical force acting on the unit area of the strip foundation is noted as $Q = qB_0$. The horizontal inertia force is noted as $F_h = k_h Q$, in which $k_h$ is the average horizontal seismic coefficient. The surface overload is divided into two parts, namely, the vertical component $q_0$ and the seismically induced component $k_h q_0$. The vertical body force, $\gamma$, was induced by gravitational acceleration, and horizontal body force, $k_h \gamma$, was induced by seismic acceleration.

The analysis considers the foundation ground roughness to be infinite, and the interface of footing rock as perfectly bonded. Damage to the structure caused by seismic wave action is the result of the compound effect of an increase in external driving force and a decrease in the shear resistance of the rock foundation. In addition, the focus of the study was the strength of the foundation, without considering the effect of seismic loading on the stability of the foundation.

### 2.2. Modified HB Failure Criterion

It has been demonstrated that the damage envelope of rock foundations in $\sigma - \tau$ stress space is not linear [28], and the direct application of linear MC criterion will lead to a great deviation. Therefore, the foundation damage on rock mass obeying the modified HB criterion is investigated in this manuscript. The modified HB criterion introduced by Yang and Yin [12] is adopted in the analysis, which is given as follows:

$$\sigma_1 - \sigma_3 = \sigma_c \left[ \frac{m\sigma_3}{\sigma_c} + s \right]^n \tag{2}$$

where $\sigma_1$ and $\sigma_3$ are the major and minor principal stresses, respectively, and $\sigma_c$ is the uniaxial compressive stress during rock failure. The parameters $m$, $s$, and $n$ were defined by Hoek et al. [19], which are calculated as follows:

$$\frac{m}{m_i} = exp\left( \frac{GSI - 100}{28 - 14D} \right) \tag{3}$$

$$s = exp\left( \frac{GSI - 100}{9 - 3D} \right) \tag{4}$$

$$n = \frac{1}{2} + \frac{1}{6}\left[ exp\left( -\frac{GSI}{15} \right) - exp\left( -\frac{20}{3} \right) \right] \tag{5}$$

where $GSI$ is the Geological Strength Index characterizing the quality of the rock mass, and its value range is generally 10–80; $D$ is the disturbance coefficient of the intact rock mass, and its variation range is from 0.0 for intact rock mass to 1.0 for strongly disturbed rock mass; and $m_i$ is the m-value of the intact rock mass with a variation range of 4 to 33, which is generally obtained by experiment. It should be noted that the upper limits of $m_i$ correspond to coarse igneous rocks such as granite, while the lower limits correspond to very weak rocks such as clay rocks. The approximate $m_i$ values of five types of rocks proposed by Hoek [18,19] were selected in the analysis as parameters for discussion, which include 22 (intense shear zones), 20 (brecciated shear/faults), 15.5 (sericite with low quartz), 14 (sericite with similar quartz), and 25 (sericite with high quartz). More $m_i$ values for typical rocks listed in the literature [18] were used for replacement in subsequent studies.

*2.3. Generalized Tangent Method*

In the upper limit analysis, a linear yield surface, as an externally tangent of the real nonlinear damage envelope, was selected to evaluate the actual load, which is called the generalized tangent technique [15,16], and is shown in Figure 2. It can be seen in Figure 2 that the strength of the tangent line is greater than that of the nonlinear HB failure criterion for the same positive stress. Therefore, the material ultimate load obtained from the tangent line gives the upper limit of the actual ultimate load of the material that conforms to the nonlinear HB criterion. In the following analysis, instead of using the nonlinear HB criterion in Equation (1), the linear equivalent MC criterion in Equation (6) is used to calculate the external power and internal energy dissipation rate. The tangent line of the nonlinear HB destruction criterion at the point M is shown in Figure 2, which is described by the following equation:

$$\tau = c_t + \sigma_n \tan\varphi_t \tag{6}$$

where $\varphi_t$ is the equivalent tangential friction angle, and $c_t$ is the intercept of the tangent line on the τ axis. The relationship between $\varphi_t$ and $c_t$ is given as follows [12]:

$$\frac{c_t}{\sigma_c} = \frac{\cos\varphi_t}{2}\left[\frac{mn(1-\sin\varphi_t)}{2\sin\varphi_t}\right]^{\frac{n}{1-n}} - \frac{\tan\varphi_t}{m}\left(1+\frac{\sin\varphi_t}{n}\right)\left[\frac{mn(1-\sin\varphi_t)}{2\sin\varphi_t}\right]^{\frac{1}{1-n}} + \frac{s}{m}\tan\varphi_t \tag{7}$$

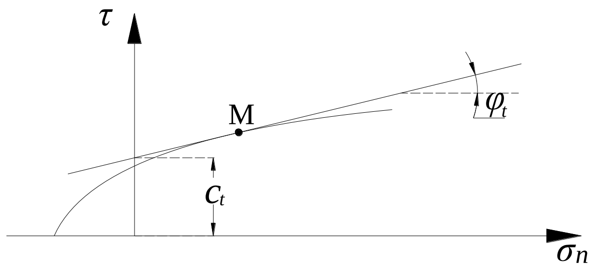


**Figure 2.** Tangential line for modified HB failure criterion.

The equivalent cohesion, $c_t$, corresponding to different equivalent friction angles, $\varphi_t$, can be obtained by using the generalized tangent technique. In the following, the seismic bearing capacity of a strip foundation placed on the surface of a rock mass will be evaluated using the generalized Prandtl mechanism.

## 3. Kinematic Analysis of Strip Foundation on Rock Foundation under Seismic Action

The rock mass considered in the analysis obeyed the modified HB failure criterion, which was simplified by using the generalized tangent technique. The inertia forces caused by seismic motion was also taken into consideration to investigate its effect on the ultimate bearing capacity of foundation. It has been shown [24] that the kinematic analysis of structures is an effective method for solving the upper limit of the bearing capacity. The upper limit theorem shows that in any kinematically allowed virtual velocity field (the field is compatible with the velocity at the boundary of the rock mass), the rate of work done by the actual external forces is less than or equal to the rate of internal energy dissipation within the rock and soil mass itself due to friction. The power of external force considered in the following analysis includes the vertical load on the foundation, the ground overload, the inertia force of the weight of the rock mass, and the earthquake acceleration. After loading, the work done by the frictional force on the velocity discontinuity surface inside the rock causes the internal energy to be consumed to balance the work done by the external force. Meanwhile, in order to obtain the smallest upper limit solution, it is necessary to simulate as many kinematically allowed velocity fields as possible. The analysis was performed in this study using a generalized Prandtl failure mechanism to find the smallest possible upper bound solution using multiple optimizations.

The seismic effect of a strip foundation placed on the surface of a rock foundation ($D$ = 0) is analyzed in the following section considering a case corresponding to the classical problem of a shallow foundation on a semi-infinite horizontal rock medium.

### *3.1. Generalized Prandtl Failure Mechanism*

The Prandtl failure mechanism is extended to rock foundations obeying the modified HB criterion, as shown in Figure 3. As the seismic action is considered in the analysis, there is a tendency toward movement to the right in the horizontal direction.

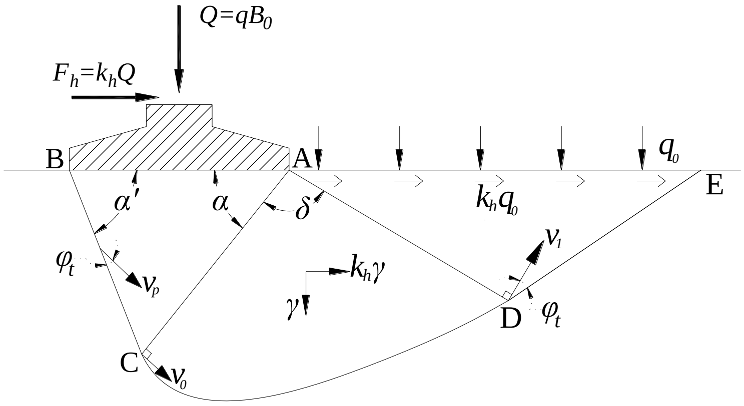


**Figure 3.** Generalized Prandtl failure mechanism.

The right side of failure mechanism consists of three parts, which include:

- The rigid wedge ABC (defined by the angular parameters $\alpha$, $\alpha'$) under the base of the foundation with velocity, $v_p$ along the direction at an angle of $\varphi_t$ with BC for rigid body motion.
- The sector ACD (defined by the angle $\delta$) delineated by the logarithmic helix CD with A as the focal point, the side length of logarithmic helix shear zone is $AD = ACe^{\delta \tan \varphi_t}$, where the length of AC is $r_0 = B_0 \frac{\sin \alpha'}{\sin(\alpha+\alpha')}$. The velocity increases exponentially from $v_0 = v_p \frac{\sin(\alpha+\alpha'-2\varphi_t)}{\cos \varphi_t}$ on the AC side so that $v_1 = v_0 e^{\delta \tan \varphi_t}$ on the AD side.
- The rigid wedge ADE in the rock masses on the side of the foundation, which carries out rigid body motion along the direction of angle $\varphi_t$ with the velocity $v_1$.
- The rest of the rock body remains stationary.

### *3.2. Calculation of Work Done by External Forces*

As the rock mass below the edge of the body BCDE shown in Figure 3 remains stationary, BCDE is a velocity interruption line. According to the flow law, the velocity of each point along this line must be at an angle of $\varphi_t$ with the line. Since AC is a velocity interruption line, the velocity $v_0$ (velocity of the rock masses at the right of AC) is perpendicular to AC, when the body moves. Therefore, the value of $v_0$ is $v_p \frac{\sin(\alpha+\alpha'-2\varphi_t)}{\cos \varphi_t}$, and $v_{p0}$, the change of velocity vector across AC, is at an angle of $\varphi_t$ with AC. The compatible velocity diagram at AC is shown in Figure 4. AD is not a velocity interruption line, so the motion of rigid wedge ADE and the sector area ACD can be kept continuous, and the wedge ADE will be rigidly translated with velocity $v_1$. The velocity vector triangle consisting of $v_p$, $v_{p0}$, and $v_0$ mentioned in this paragraph and the direction of $v_1$ are shown in Figure 4.

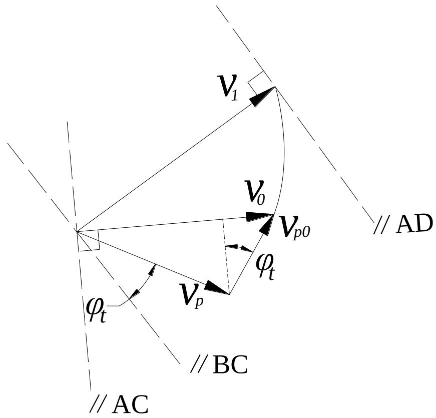


**Figure 4.** Velocity compatibility schematic.

The work done by external forces in assumed failure mechanism includes the self-weight action of the rock mass, $\gamma$; the vertical load, $Q$, borne by the foundation; the surface overload, $q_0$; and the related pseudo-static inertia force simplified by the seismic action. Since the effect of vertical seismic acceleration is ignored in this consideration, therefore, the work done by the external forces include:

(1) work done by the vertical load, $Q$:

$$W_{e1} = Qv_p\left[\sin\left(\alpha' - \varphi_t\right) + k_h \cos\left(\alpha' - \varphi_t\right)\right] \tag{8}$$

(2) work done by rock mass gravity, $\gamma$:

$$\begin{aligned} W_{e2} = &\left\{ \frac{\gamma B_0^2 \sin\alpha' \sin\alpha}{2\sin(\alpha+\alpha')} \cdot v_p \sin(\alpha' - \varphi_t) \right\} \\ &+ \left\{ \frac{\gamma}{2} \cdot v_p \frac{\sin(\alpha+\alpha'-2\varphi_t)}{\cos\varphi_t} \cdot \left( B_0 \frac{\sin\alpha'}{\sin(\alpha+\alpha')} \right)^2 \cdot \frac{[3\tan\varphi_t \cos(\alpha+\delta) + \sin(\alpha+\delta)]e^{3\delta\tan\varphi_t} - \sin\alpha - 3\tan\varphi_t\cos\alpha}{9tan^2\varphi_t + 1} \right\} \\ &+ \left\{ -\frac{\gamma}{4} \cdot \left( B_0 \frac{\sin\alpha'}{\sin(\alpha+\alpha')} \right)^2 \cdot e^{3\delta\tan\varphi_t} \sin 2(\alpha+\delta) \cdot v_p \frac{\sin(\alpha+\alpha'-2\varphi_t)}{\cos(\alpha+\delta-\varphi_t)} \right\} + \left\{ k_h \frac{\gamma B_0^2 \sin\alpha' \sin\alpha}{2\sin(\alpha+\alpha')} \cdot v_p \cos\left(\alpha'^{-\varphi_t}\right) \right\} \\ &+ \left\{ k_h \frac{\gamma}{2} \cdot v_p \frac{\sin(\alpha+\alpha'-2\varphi_t)}{\cos\varphi_t} \cdot \left( B_0 \frac{\sin\alpha'}{\sin(\alpha+\alpha')} \right)^2 \cdot \frac{[3\tan\varphi_t \sin(\alpha+\delta) - \cos(\alpha+\delta)]e^{3\delta\tan\varphi_t} + \cos\alpha - 3\tan\varphi_t\sin\alpha}{9tan^2\varphi_t + 1} \right\} \\ &+ \left\{ -k_h \frac{\gamma}{2} \cdot \left( B_0 \frac{\sin\alpha'}{\sin(\alpha+\alpha')} \right)^2 e^{3\delta\tan\varphi_t} \sin^2(\alpha+\delta) \cdot v_p \frac{\sin(\alpha+\alpha'-2\varphi_t)}{\cos(\alpha+\delta-\varphi_t)} \right\} \end{aligned} \tag{9}$$

(3) work done by surface overload, $q_0$:

$$\begin{aligned} W_{e3} = &\left\{ -q_0 \cdot B_0 \frac{\sin\alpha'}{\sin(\alpha+\alpha')} \cdot v_p \frac{\sin(\alpha+\alpha'-2\varphi_t)}{\cos\varphi_t} \cdot \frac{\cos\varphi_t \cos(\alpha+\delta)}{\cos(\alpha+\delta-\varphi_t)} e^{2\delta\tan\varphi_t} \right\} \\ &+ \left\{ -k_h \cdot q_0 \cdot B_0 \frac{\sin\alpha'}{\sin(\alpha+\alpha')} \cdot v_p \frac{\sin(\alpha+\alpha'-2\varphi_t)}{\cos\varphi_t} \cdot \frac{\cos\varphi_t \sin(\alpha+\delta)}{\cos(\alpha+\delta-\varphi_t)} e^{2\delta\tan\varphi_t} \right\} \end{aligned} \tag{10}$$

Then the total work done by the external forces applied to the mechanism can be written as:

$$W_e = Qv_p\left[\sin\left(\alpha' - \varphi_t\right) + k_h\cos\left(\alpha' - \varphi_t\right)\right] + \frac{\gamma v_p B_0^2}{2}\left[(f_1 + f_2 + f_3) + k_h\left(f_1' + f_2' + f_3'\right)\right] + q_0 v_p B_0\left(f_4 + k_h f_4'\right); \tag{11}$$

where $f_1$, $f_2$, $f_3$, $f_4$, $f_1'$, $f_2'$, $f_3'$, and $f_4'$ are the functions of the angle parameters $\alpha$, $\alpha'$, $\delta$, and $\varphi_t$, which are shown here:

$$f_1 = \frac{\sin\alpha' \sin\alpha}{\sin(\alpha + \alpha')} \sin\left(\alpha' - \varphi_t\right); \tag{12}$$

$$f_2 = \frac{\sin(\alpha+\alpha'-2\varphi_t)}{\cos\varphi_t}\cdot\left(\frac{\sin\alpha'}{\sin(\alpha+\alpha')}\right)^2\cdot\frac{[3\tan\varphi_t\cos(\alpha+\delta)+\sin(\alpha+\delta)]e^{3\delta\tan\varphi_t}-\sin\alpha-3\tan\varphi_t\cos\alpha}{9tan^2\varphi_t+1}; \tag{13}$$

$$f_3 = -\frac{1}{2}\left(\frac{\sin\alpha'}{\sin(\alpha+\alpha')}\right)^2\cdot e^{3\delta\tan\varphi_t}\sin 2(\alpha+\delta)\cdot\frac{\sin(\alpha+\alpha'-2\varphi_t)}{\cos(\alpha+\delta-\varphi_t)}; \tag{14}$$

$$f_4 = -\frac{\sin\alpha'}{\sin(\alpha+\alpha')}\cdot\frac{\sin(\alpha+\alpha'-2\varphi_t)}{\cos\varphi_t}\cdot\frac{\cos\varphi_t\cos(\alpha+\delta)}{\cos(\alpha+\delta-\varphi_t)}e^{2\delta\tan\varphi_t}; \tag{15}$$

$$f_1' = \frac{\sin\alpha'\sin\alpha}{\sin(\alpha+\alpha')}\cdot\cos(\alpha'-\varphi_t); \tag{16}$$

$$f_2' = \frac{\sin(\alpha+\alpha'-2\varphi_t)}{\cos\varphi_t}\cdot\left(\frac{\sin\alpha'}{\sin(\alpha+\alpha')}\right)^2\cdot\frac{[3\tan\varphi_t\sin(\alpha+\delta)-\cos(\alpha+\delta)]e^{3\delta\tan\varphi_t}+\cos\alpha-3\tan\varphi_t\sin\alpha}{9tan^2\varphi_t+1}; \tag{17}$$

$$f_3' = -\left(\frac{\sin\alpha'}{\sin(\alpha+\alpha')}\right)^2\cdot e^{3\delta\tan\varphi_t}\ \sin^2(\alpha+\delta)\cdot\frac{\sin(\alpha+\alpha'-2\varphi_t)}{\cos(\alpha+\delta-\varphi_t)}; \tag{18}$$

$$f_4' = -\frac{\sin\alpha'}{\sin(\alpha+\alpha')}\cdot\frac{\sin(\alpha+\alpha'-2\varphi_t)}{\cos\varphi_t}\cdot\frac{\cos\varphi_t\sin(\alpha+\delta)}{\cos(\alpha+\delta-\varphi_t)}e^{2\delta\tan\varphi_t}; \tag{19}$$

The functions $f_1$, $f_2$, and $f_3$ reflect the influence of the unit weight of rock mass; function $f_4$ reflects the influence of surface overload; functions $f_1'$, $f_2'$, $f_3'$, and $f_4'$ reflect the influence of the horizontal seismic acceleration.

### 3.3. Calculation of Internal Energy Consumption

As the internal energy dissipation in the mechanism comes from the velocity jump on the velocity interruption lines BC, AC, CD, DE, and the shear energy dissipation inside the sector area ACD, the internal frictional resistance of the mechanism consists of:

(1) shear energy dissipation inside the rock mass:

$$W_{i1} = \frac{1}{2}c_t v_p\frac{\sin(\alpha+\alpha'-2\varphi_t)}{\cos\varphi_t}B_0\frac{\sin\alpha'}{\sin(\alpha+\alpha')}\frac{e^{2\delta\tan\varphi_t}-1}{\tan\varphi_t}; \tag{20}$$

(2) energy dissipation for velocity discontinuity on the velocity discontinuity line BC:

$$W_{i2} = c_t v_p B_0\cos\varphi_t\frac{\sin\alpha}{\sin(\alpha+\alpha')}. \tag{21}$$

(3) energy dissipation for velocity discontinuity on velocity interruption line AC:

$$W_{i3} = -c_t v_p B_0\frac{\sin\alpha'}{\sin(\alpha+\alpha')}\cos(\alpha+\alpha'-\varphi_t). \tag{22}$$

(4) energy dissipation for velocity discontinuity on velocity discontinuity line CD:

$$W_{i4} = \frac{1}{2}c_t v_p\frac{\sin(\alpha+\alpha'-2\varphi_t)}{\cos\varphi_t}B_0\frac{\sin\alpha'}{\sin(\alpha+\alpha')}\frac{e^{2\delta\tan\varphi_t}-1}{\tan\varphi_t}; \tag{23}$$

(5) energy dissipation for velocity discontinuity on the velocity interrupted line DE:

$$W_{i5} = -c_t v_p B_0\sin(\alpha+\alpha'-2\varphi_t)\frac{\sin\alpha'}{\sin(\alpha+\alpha')}\frac{\sin(\alpha+\delta)}{\cos(\alpha+\delta-\varphi_t)}e^{2\delta\tan\varphi_t} \tag{24}$$

Finally, the internal energy dissipation rate of the failure mechanism can thus be rewritten as:

$$W_i = c_t v_p B_0(g_1+g_2+g_3+g_4); \tag{25}$$

where $g_1$, $g_2$, $g_3$, and $g_4$ are the functions of the angle parameters $\alpha$, $\alpha'$, $\delta$, and $\varphi_t$, which can be calculated as:

$$g_1 = \frac{\sin(\alpha+\alpha'-2\varphi_t)}{\cos\varphi_t}\cdot\frac{\sin\alpha'}{\sin(\alpha+\alpha')}\cdot\frac{e^{2\delta\tan\varphi_t}-1}{\tan\varphi_t} \tag{26}$$

$$g_2 = \cos\varphi_t\frac{\sin\alpha}{\sin(\alpha+\alpha')}; \tag{27}$$

$$g_3 = -\frac{\sin\alpha'}{\sin(\alpha+\alpha')}\cos(\alpha+\alpha'-\varphi_t). \tag{28}$$

$$g_4 = -\sin(\alpha+\alpha'-2\varphi_t)\frac{\sin\alpha'}{\sin(\alpha+\alpha')}\frac{\sin(\alpha+\delta)}{\cos(\alpha+\delta-\varphi_t)}e^{2\delta\tan\varphi_t}; \tag{29}$$

### *3.4. Calculation of Upper Bound of Mechanism Bearing Capacity*

The work done by the external force on the mechanism and the energy consumed internally by the drag force are expressed in this subsection as functions of four angles: $\alpha$, $\alpha'$, $\delta$, and $\varphi_t$, which are $\{f_1, f_2, f_3, f_4, f_1', f_2', f_3', f_4'\}$ and $\{g_1, g_2, g_{3,}g_4\}$. According to the geometry in Figure 3, the range of values for the four angular parameters is limited to $\frac{\pi}{2} < \alpha+\alpha'-\varphi_t < \pi$. $0 < \alpha, \alpha', \varphi_t, \delta < \frac{\pi}{2}$. $0 < \alpha'-\varphi_t < \frac{\pi}{2}$. $\frac{\pi}{2}+\varphi_t < \alpha+\delta < \pi$.

An upper limit of the upper load, $q$, that can be carried by the strip foundation located on the surface of the rock mass under the influence of seismic acceleration in the Prandtl failure mechanism is then expressed as:

$$q \le q_u = \min_{\alpha,\alpha',\delta,\varphi_t}\frac{c_t G - 0.5B_0\gamma F_1 - q_0 F_2}{\sin(\alpha'-\varphi_t)+k_h\cos(\alpha'-\varphi_t)} \tag{30}$$

where $G = \sum_{i=1}^{4} g_i$; $F_1 = (f_1+f_2+f_3)+k_h(f_1'+f_2'+f_3')$; and $F_2 = f_4 + k_h f_4'$.

The upper bound, $q_u$, of the bearing capacity of strip foundation could obtained by adjusting the three control angle parameters of failure mechanism $\alpha$, $\alpha'$, $\delta$.

The calculation process in this section can be illustrated by Figure 5:

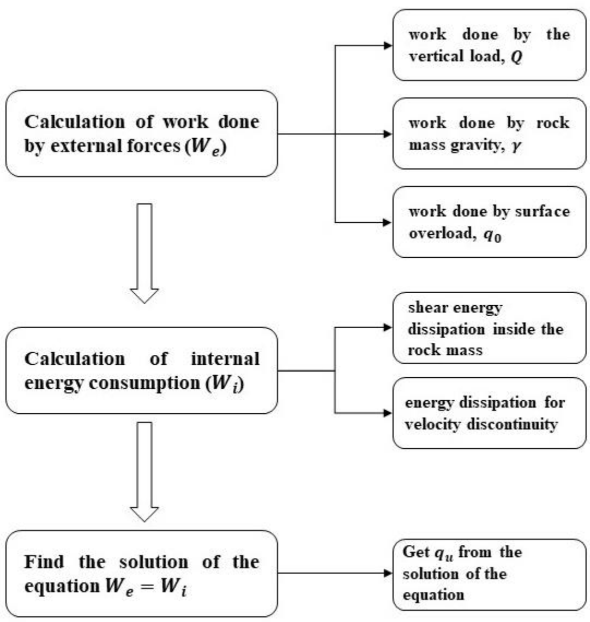


**Figure 5.** Calculation process of $q_u$.

## 4. Verification

Verification of the present work was carried out in two parts. In Section 4.1, a comparison with the analytical results of Yang and Yin [12] is first presented. In Section 4.2, the ultimate bearing capacity of strip foundations placed on five typical rock masses is calculated using this method, and the calculated results are compared with those of the finite element model.

### *4.1. Verification against Existing Theoretical Results (Analytical Solutions)*

The estimation of the upper limit of the ultimate bearing capacity of a strip foundation on a rock foundation, such as conducted in studies by Yang and Yin [12] and Saada [27], is usually based on the assumption of a multi-wedge body failure mechanism. The control parameters of such mechanisms include the angle parameter, $\theta$, of the rigid body under the foundation; the top angle, $\alpha_i$, and bottom angle, $\beta_i$, of each wedge; and the equivalent friction angle, $\varphi_t$, which represents the nature of the rock mass itself. The computational accuracy of such mechanisms is mainly determined by the total number of divided wedges, $k$. To demonstrate the validity of the assessment method based on the generalized Prandtl mechanism provided in this study, a hypothetical failure mechanism with $GSI = 30$, $m_i = 17$, $D = 0$, $\sigma_c = 10$ MPa , $\gamma = 22$ kN/m$^3$, and $B_0 = 1.0$ m was selected without considering the seismic effect (assuming $k_h = 0$), and the trend of the upper limit of the bearing capacity with the variation of $q_0$ was demonstrated and then compared with the experimental results of Yang and Yin [12]. The comparison results are shown in Table 1.

**Table 1.** Comparison of the calculated results of this study with those of Yang and Yin [12].

| **Bearing Capacity $q_0$ (kPa)** | 10 | 20 | 30 | 40 |
|---|---|---|---|---|
| Results of Yang and Yin (MPa) | 14.383 | 14.568 | 14.745 | 14.914 |
| Results of present work (MPa) | 14.684 | 15.707 | 16.099 | 16.492 |
| Error (%) | 2.05 | 7.25 | 8.42 | 9.57 |

Table 1 shows that the ultimate bearing capacity calculated by the present method is larger relative to the upper bound estimate of the bearing capacity of Yang and Yin [12]. The maximum error does not exceed 10%, which indicates that the upper bound estimate of the bearing capacity in this paper is reliable. The reason for this discrepancy is that the equivalent friction angle selection method recommended by Drescher and Christopoulos [25] and Collins et al. [26] was adopted in the study by Yang and Yin [12], while the equivalent $c_t$ and $\varphi_t$ calculation methods summarized by Hoek [18,19] based on practical engineering experience were chosen here.

This equivalence friction angle generation, conducted by fitting the nonlinear HB damage criterion envelope, was used in the analysis of the present work to solve Equation (2), as recommended by Evert Hoek et al. [18,19]. The purpose of adapting this process was mainly to balance the area of the nonlinear HB curve above and below the linear MC envelope, so that one could find the fitting line that can best represent the change trend of HB strength envelope:

$$\varphi_t = \sin^{-1}\left[\frac{6nm(s+m\sigma_{3n})^{n-1}}{2(1+n)(2+n)+6nm(s+m\sigma_{3n})^{n-1}}\right] \tag{31}$$

in which $\sigma_{3n} = \frac{\sigma_{3max}}{\sigma_c}$, and:

$$\frac{\sigma_{3max}}{\sigma_{cm}} = 0.47\left(\frac{\sigma_{cm}}{\gamma H}\right)^{-0.94} \tag{32}$$

$$\sigma_{cm} = \sigma_c \frac{[m+4s-n(m-8s)]\left(\frac{m}{4}+s\right)^{n-1}}{2(1+n)(2+n)} \tag{33}$$

where $H$ is the depth of layer, which is assumed to be 100 m in this study.

Since the equivalent MC envelope is always on the upper side of the nonlinear HB failure envelope, the equivalent friction angle, $\varphi_t$, and equivalent cohesive force, $c_t$, determined by the equivalent MC envelope, can be used to solve the upper limit of bearing capacity. In the following calculation process, the values of $\varphi_t$ and $c_t$ do not change, ensuring that the equivalent friction angle, $\varphi_t$, is always the angle that represents the direction of the HB criterion envelope. In the following calculation, by changing the shape of the failure mechanism itself (namely, adjusting the three control angle parameters, $\alpha'$, $\alpha$, and $\delta$), the minimum of the upper bound of the ultimate bearing capacity can be found.

One advantage of this method is that the minimization process of ultimate bearing capacity is accomplished by changing the shape of the mechanism itself. The method can find the equivalent friction angle, $\varphi_t$, and the corresponding equivalent cohesive force, $c_t$, which best represent the characteristics of the rock mass after determining the type of rock mass (namely, determining the rock mass parameters $GSI$, $m_i$, and $\sigma_c$).

### 4.2. Verification against Numerical Analysis Results

Different rock masses have unique mechanical characteristics, and the HB criterion uses the parameters $GSI$, $D$, and $m_i$ to describe the characteristics of different rocks. In the following, five typical rocks provided by Hoek [18,19] were selected as examples to seek the supremum (the minimum values of the upper limit) of the ultimate bearing capacity, and the corresponding failure mechanisms when the supremum is obtained are shown in Table 2. More parameters for typical rocks are provided in the literature [18] for reference. The results presented in this section are the supremum of the bearing capacity without considering overload and seismic action ($q_0 = 0$, $k_h = 0$). Since only the load carrying capacity calculation case cited in the previous section was carried out in Yang and Yin's study [12], the predicted results in this section will be compared with the numerical calculation results of the ABAQUS finite element model.

**Table 2.** The parameters and upper limit of ultimate bearing capacity of five typical rocks.

| No. | Rock Mass Properties | $\sigma_c$ (MPa) | GSI | $D$ | $m_i$ | $q_{u,analysis}$ (MPa) | $q_{u,numerical}$ (MPa) | $\Delta q$ (MPa) | Error (%) |
|---|---|---|---|---|---|---|---|---|---|
| I | Intense shear zones | 7.5 | 25 | 0 | 22 | 11.43 | 11.10 | 0.33 | 2.9 |
| II | Brecciated shear/faults | 25 | 25 | 0 | 20 | 38.35 | 37.57 | 0.78 | 2.0 |
| III | Sericite with low quartz | 20 | 34 | 0 | 15.5 | 35.85 | 35.62 | 0.23 | 0.6 |
| IV | Sericite with similar quartz | 40 | 47 | 0 | 14 | 170.30 | 163.48 | 6.82 | 4.0 |
| V | Sericite with high quartz | 60 | 60 | 0 | 25 | 216.36 | 214.76 | 1.6 | 0.7 |

As shown in Figure 6, this model is a simulation of the ultimate load of a strip foundation on a rock mass. The width of the strip foundation was $B$ = 0.5 m, and to eliminate the influence of size effect, the foundation was therefore set as a 5 m × 5 m square rock mass. The model had 918 nodes, 845 elements, and the element type was CPE4. The size of the rock unit decreases as the distance from the base of the bar increases. In the X direction (horizontal), the unit size increases from left to right with a minimum of 0.05 m (left) and a maximum of 0.5 m (right). In the Y direction (vertical), the unit size increases from top to bottom with a minimum of 0.05 m (top) and a maximum of 0.5 m (bottom). The ultimate bearing capacity obtained from each numerical simulation is given in the following table. When comparing the prediction results of this study with the numerical simulation results, the error between them is less than 5%.

The failure mechanisms corresponding with the supremum of the ultimate bearing capacity on the same kind of rock (with the same $GSI$, $D$, and $m_i$) remain unchanged when the consideration of overload and seismic action is added in the subsequent sections. The critical failure surfaces for different rock mass are shown in Figures 7–12.

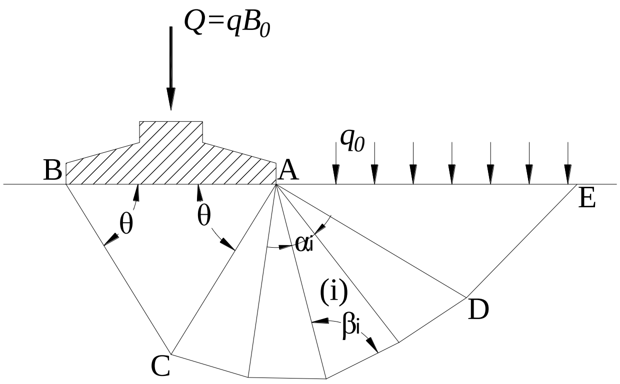


**Figure 6.** Multi-wedge failure mechanism commonly used in research by Yang and Yin [12].

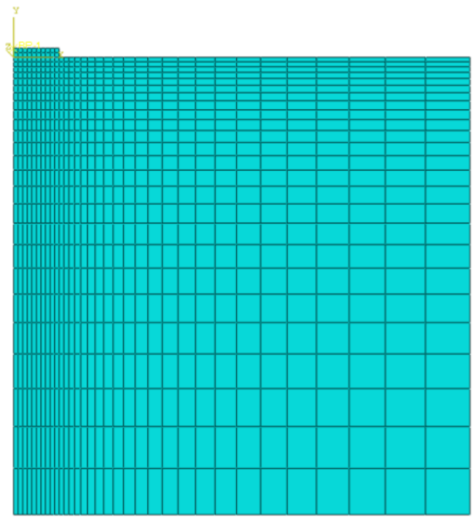

**Figure 7.** Finite element model meshing in ABAQUS.

I Intense shear zones

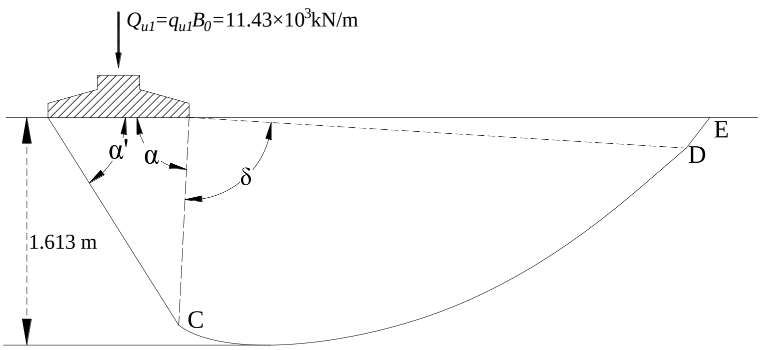


**Figure 8.** Critical failure surface ($\varphi_t = 34.33°;\ \alpha' = 57.82°;\ \alpha = 87.14°;\ \delta = 89.33°$).

II Brecciated shear/faults

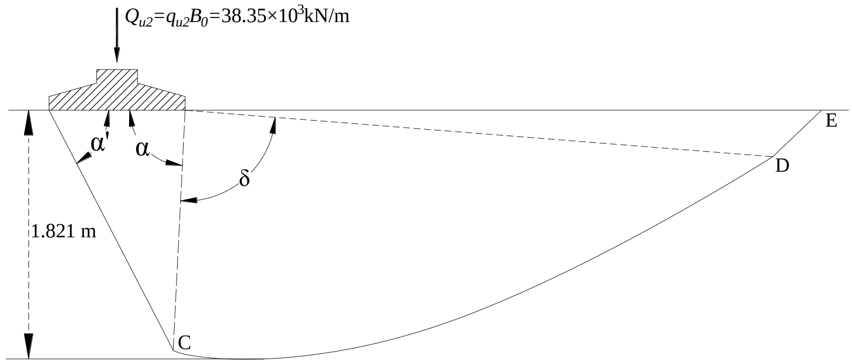


**Figure 9.** Critical failure surface ($\varphi_t = 41.93°$; $\alpha' = 62.56°$; $\alpha = 87.14°$; $\delta = 88.34°$).

III Sericite with low quartz

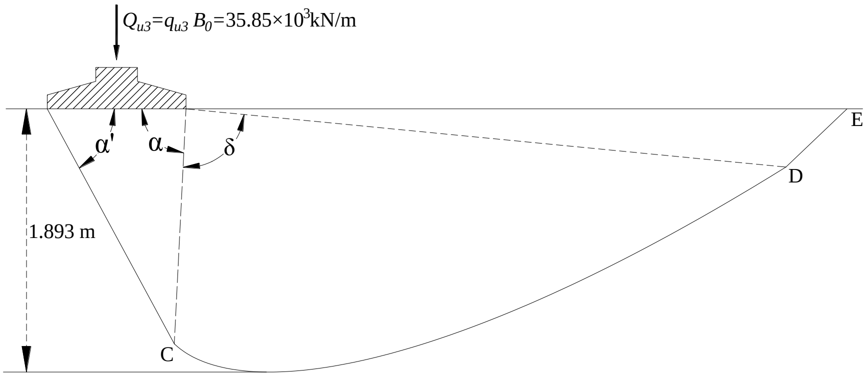


**Figure 10.** Critical failure surface ($\varphi_t = 40.92°$; $\alpha' = 61.55°$; $\alpha = 87.14°$; $\delta = 87.33°$).

IV Sericite with similar quartz

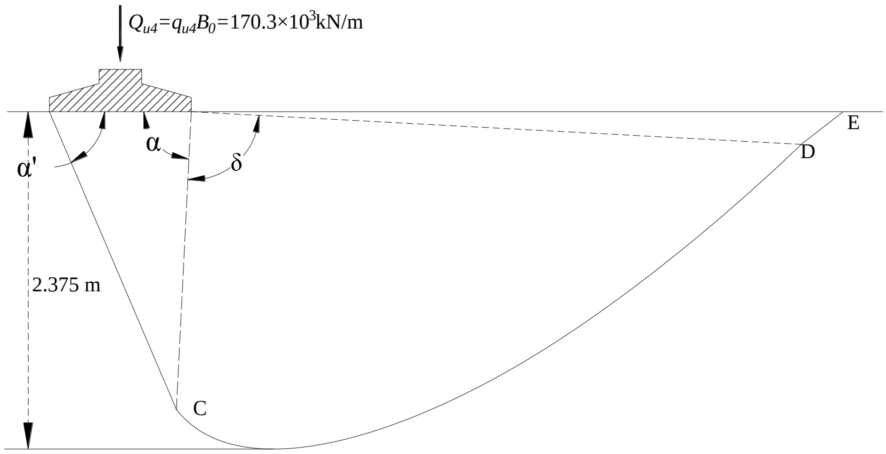


**Figure 11.** Critical failure surface ($\varphi_t = 49.12°$; $\alpha' = 66.89°$; $\alpha = 87.14°$; $\delta = 89.80°$).

V Sericite with high quartz

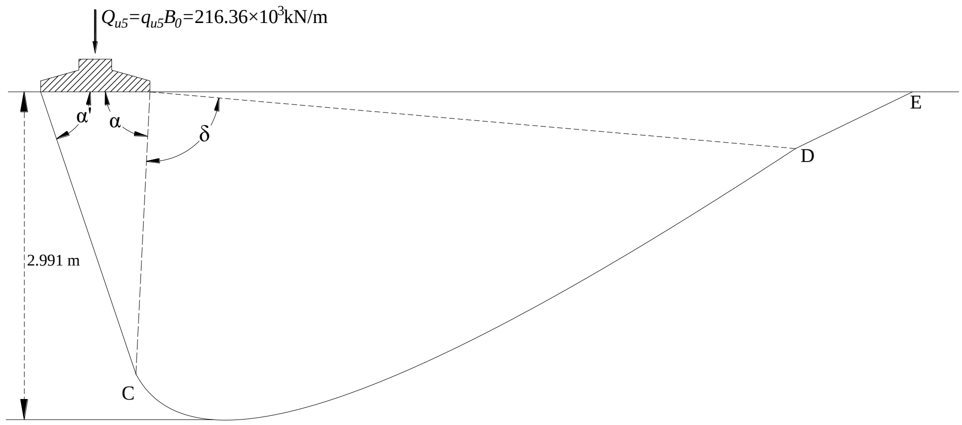


**Figure 12.** Critical failure surface ($\varphi_t = 59.24°;\ \alpha' = 71.27°;\ \alpha = 87.14°;\ \delta = 88.46°$).

A large GSI value (>25) indicates a high quality rock mass, while a larger $m_i$ denotes a stronger and more complete rock mass. Therefore, sample I is a poor quality rock mass, while II and III have relatively similar strength and rock mass, and samples IV and V have very good rock integrity and very high quality. As can be seen from the table, the bearing capacity results predicted in this study match the rock masses of the samples.

Comparing the failure mechanisms of the five types of rock masses, it can be determined that:

1. The calculated value of the equivalent friction angle, $\varphi_t$, is greater for rock masses with good properties, and the ultimate bearing capacity increases with an increase in $\varphi_t$.
2. The shapes of the slip surfaces of different masses are similar when reaching the failure, but with the increase in ultimate bearing capacity that can be provided, the depth of the mobilized rock mass increases and the overall volume increases.
3. The angular parameters of the failure mechanism can basically be determined within a general range: the range of values for $\alpha'$ can be set at 55° to 70°, the better the rock mass, the larger the value taken; $\alpha$ can be set at 87°; and $\delta$ can be set at 90°. The shape of the damage mechanism of the rock foundation can be roughly depicted using this set of parameters.

## 5. Parametric Analysis

This section focuses on the effects of surface overload, $q_0$, rock self-weight, $\gamma$, and horizontal seismic coefficient, $k_h$, on the seismic bearing capacity of the foundation. The conclusion is consistent with the existing results [6]; that is, the elevation of the surface overload and the self-weight of the rock mass is beneficial for improving the ultimate bearing capacity of the foundation, while an increase in the horizontal seismic coefficient will lead to a sharp decrease in the bearing capacity.

### *5.1. Effect of Surface Overload, $q_0$, and Rock Mass Gravity, $\gamma$*

The effects of surface overload, $q_0$, and rock mass gravity, $\gamma$, on the upper limit of bearing capacity, $q_u$, was investigated on a rock mass much like the intense shear zones above, where $\sigma_c = 7.5$ MPa, $GSI = 25$, $D = 0$, and $m_i = 22$.

The variation trend of the upper limit of ultimate bearing capacity of foundations when $q_0$ changes from 0–50 kPa (fixed $\gamma = 23.1$ kN/m$^3$) was first studied. Figure 13 shows the variation of the upper limit with surface overload, $q_0$, in the static case ($k_h = 0$) and the seismic case ($k_h = 0.1$). The results were as expected: the ultimate bearing capacity of the foundation decreases under the seismic action. Inspection of Figure 13 suggests that the decrease in bearing capacity during the earthquake was significant and became more dramatic with an increase in the surface overload, $q_0$. Table 3 shows the differences between the estimated upper limit of the bearing capacity for the static case ($k_h = 0$) and the earthquake case ($k_h = 0.1$).

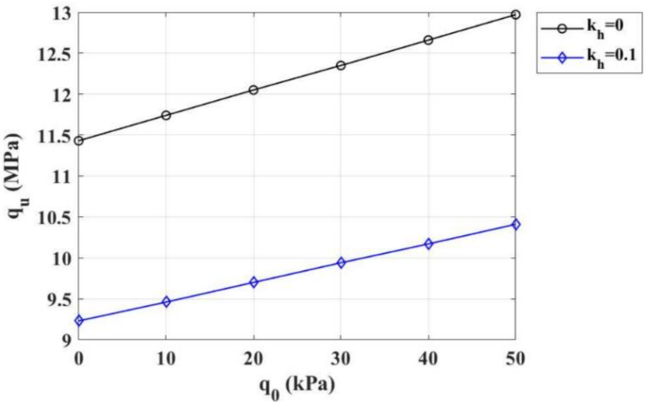


**Figure 13.** Effect of surface overload, $q_0$, on the upper limit of ultimate bearing capacity, $q_u$.

**Table 3.** Upper bound of ultimate bearing capacity under different seismic intensities.

| $q_0$ (kPa) | $q_u$ (MPa) | | $\Delta q_u$ |
|---|---|---|---|
| | $k_h$ = 0 | $k_h$ = 0.1 | |
| 0 | 11.43 | 9.23 | 2.20 |
| 10 | 11.74 | 9.46 | 2.28 |
| 20 | 12.05 | 9.70 | 2.35 |
| 30 | 12.35 | 9.94 | 2.41 |
| 40 | 12.66 | 10.17 | 2.49 |
| 50 | 12.97 | 10.41 | 2.56 |

As can be seen in Figure 14, the effect of the unit weight, $\gamma$, was lower compared to the effect of the surface overload, $q_0$, on the bearing capacity, which is also consistent with the results of a study by Saada [27]. For the determined overload, $q_0$, the unit weight, $\gamma$, rose from 20 kN/m$^3$ to 24 kN/m$^3$, while the ultimate bearing capacity rose by less than 0.1 MPa. Meanwhile for the determined unit weight, $\gamma$, every 10 kPa rise in the value of the surface overload caused the ultimate bearing capacity to rise by 0.25 MPa.

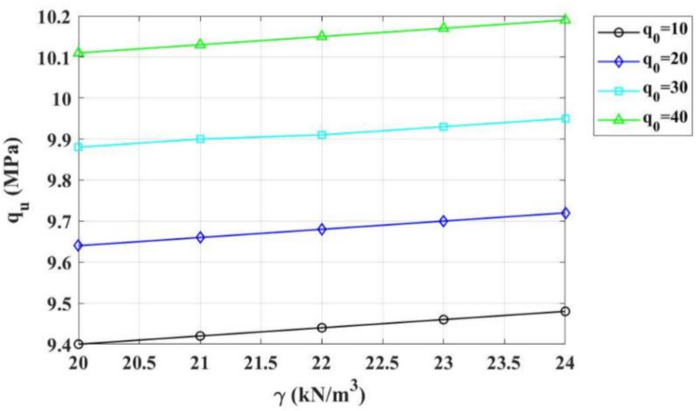


**Figure 14.** Effect of rock mass gravity, $\gamma$, on the upper limit of ultimate bearing capacity, $q_u$.

In addition, it can also be seen in Figures 13 and 14 that the variation in the upper bound of the bearing capacity, $q_u$, exhibits a linear dependence on the surface overload, $q_0$, and the unit weight of the rock mass, $\gamma$.

### 5.2. Effect of Seismic Action and Rock Properties

The calculation of bearing capacity can be rewritten into the following form by analogy with the classical form of foundation bearing capacity of Terzaghi [12]:

$$q_u = \sqrt{s}\sigma_c N_\sigma + q_0 N_q + 0.5\gamma B_0 N_\gamma \tag{34}$$

where the dimensionless parameters $N_\sigma$, $N_q$, and $N_\gamma$ are the bearing capacity coefficients of uniaxial compressive strength of rock, surface overload, and self-weight of rock mass, respectively. To facilitate application in practical geotechnical engineering, it is further extended to allow for the surface overload, $q_0$, and the unit weight of the rock mass, $\gamma$, to not be considered.

$$q_u = \sqrt{s}\sigma_c N_\sigma \tag{35}$$

where $N'_\sigma = \sqrt{s}N_\sigma$ is defined as the seismic uniaxial compressive strength bearing capacity coefficient to further facilitate the use of the table in subsequent research. The upper limit of bearing capacity calculation formula can be reduced to $q_u = \sigma_c N'_\sigma$.

This leads to the expression for the seismic uniaxial compressive strength bearing capacity coefficient: $N'_\sigma = \frac{q_u}{\sigma_c}$. The following Tables 4–8 summarize several sets of $N'_\sigma$ values for the five types of typical intact, unweathered (taking $D$ = 0) rocks mentioned above ($m_i = 22$, 20, 15.5, 14, and 25, respectively) at different seismic strengths.

**Table 4.** Seismic bearing capacity factor $N'_\sigma$ for rock-type intense shear zones.

| GSI | $k_h$ = 0 | $k_h$ = 0.05 | $k_h$ = 0.1 | $k_h$ = 0.15 | $k_h$ = 0.2 |
|---|---|---|---|---|---|
| 5 | 0.36 | 0.33 | 0.30 | 0.27 | 0.25 |
| 10 | 0.56 | 0.51 | 0.47 | 0.42 | 0.38 |
| 15 | 0.80 | 0.73 | 0.66 | 0.60 | 0.54 |
| 20 | 1.09 | 0.99 | 0.89 | 0.80 | 0.72 |
| 25 | 1.43 | 1.30 | 1.17 | 1.05 | 0.94 |
| 30 | 1.85 | 1.67 | 1.50 | 1.34 | 1.19 |
| 35 | 2.35 | 2.12 | 1.90 | 1.69 | 1.50 |
| 40 | 2.98 | 2.67 | 2.38 | 2.12 | 1.87 |
| 45 | 3.77 | 3.37 | 2.99 | 2.65 | 2.34 |
| 50 | 4.77 | 4.25 | 3.77 | 3.32 | 2.91 |
| 55 | 6.07 | 5.39 | 4.76 | 4.18 | 3.65 |
| 60 | 7.79 | 6.89 | 6.05 | 5.30 | 4.61 |
| 65 | 10.09 | 8.87 | 7.77 | 6.77 | 5.88 |
| 70 | 13.16 | 11.53 | 10.06 | 8.73 | 7.56 |
| 75 | 17.40 | 15.19 | 13.20 | 11.42 | 9.83 |
| 80 | 23.37 | 20.32 | 17.59 | 15.12 | 12.96 |

**Table 5.** Seismic bearing capacity factor $N'_\sigma$ for rock-type brecciated shear/faults.

| GSI | $k_h$ = 0 | $k_h$ = 0.05 | $k_h$ = 0.1 | $k_h$ = 0.15 | $k_h$ = 0.2 |
|---|---|---|---|---|---|
| 5 | 0.24 | 0.22 | 0.20 | 0.18 | 0.16 |
| 10 | 0.43 | 0.39 | 0.35 | 0.31 | 0.28 |
| 15 | 0.68 | 0.61 | 0.55 | 0.49 | 0.43 |
| 20 | 1.00 | 0.90 | 0.80 | 0.71 | 0.63 |
| 25 | 1.42 | 1.26 | 1.12 | 0.99 | 0.87 |
| 30 | 1.95 | 1.73 | 1.53 | 1.34 | 1.17 |
| 35 | 2.64 | 2.33 | 2.04 | 1.78 | 1.55 |
| 40 | 3.53 | 3.10 | 2.71 | 2.35 | 2.04 |
| 45 | 4.70 | 4.11 | 3.58 | 3.10 | 2.68 |
| 50 | 6.31 | 5.49 | 4.76 | 4.10 | 3.51 |
| 55 | 8.52 | 7.38 | 6.35 | 5.44 | 4.65 |
| 60 | 11.59 | 9.97 | 8.54 | 7.29 | 6.20 |
| 65 | 15.91 | 13.63 | 11.62 | 9.87 | 8.36 |
| 70 | 22.15 | 18.89 | 16.04 | 13.57 | 11.44 |
| 75 | 31.26 | 26.54 | 22.43 | 18.90 | 15.85 |
| 80 | 44.50 | 37.61 | 31.67 | 26.50 | 22.12 |

**Table 6.** Seismic bearing capacity factor $N'_\sigma$ for rock-type sericite with low quartz.

| GSI | $k_h$ = 0 | $k_h$ = 0.05 | $k_h$ = 0.1 | $k_h$ = 0.15 | $k_h$ = 0.2 |
|---|---|---|---|---|---|
| 5 | 0.19 | 0.17 | 0.16 | 0.14 | 0.13 |
| 10 | 0.32 | 0.29 | 0.27 | 0.24 | 0.22 |
| 15 | 0.50 | 0.45 | 0.41 | 0.37 | 0.33 |
| 20 | 0.72 | 0.65 | 0.58 | 0.52 | 0.46 |
| 25 | 0.99 | 0.89 | 0.80 | 0.71 | 0.63 |
| 30 | 1.33 | 1.20 | 1.07 | 0.94 | 0.83 |
| 35 | 1.76 | 1.57 | 1.40 | 1.24 | 1.09 |
| 40 | 2.31 | 2.05 | 1.82 | 1.60 | 1.40 |
| 45 | 3.03 | 2.68 | 2.36 | 2.07 | 1.80 |
| 50 | 3.98 | 3.51 | 3.07 | 2.68 | 2.33 |
| 55 | 5.24 | 4.60 | 4.02 | 3.49 | 3.03 |
| 60 | 6.98 | 6.10 | 5.31 | 4.60 | 3.98 |
| 65 | 9.42 | 8.20 | 7.11 | 6.13 | 5.26 |
| 70 | 12.90 | 11.19 | 9.63 | 8.26 | 7.06 |

**Table 7.** Seismic bearing capacity factor $N'_\sigma$ for rock-type sericite with similar quartz.

| GSI | $k_h$ = 0 | $k_h$ = 0.05 | $k_h$ = 0.1 | $k_h$ = 0.15 | $k_h$ = 0.2 |
|---|---|---|---|---|---|
| 5 | 0.14 | 0.13 | 0.12 | 0.11 | 0.10 |
| 10 | 0.26 | 0.24 | 0.21 | 0.19 | 0.17 |
| 15 | 0.43 | 0.39 | 0.35 | 0.31 | 0.28 |
| 20 | 0.66 | 0.59 | 0.53 | 0.47 | 0.41 |
| 25 | 0.96 | 0.85 | 0.76 | 0.67 | 0.59 |
| 30 | 1.34 | 1.19 | 1.05 | 0.92 | 0.81 |
| 35 | 1.86 | 1.64 | 1.44 | 1.25 | 1.09 |
| 40 | 2.53 | 2.22 | 1.94 | 1.68 | 1.46 |
| 45 | 3.43 | 3.00 | 2.61 | 2.26 | 1.95 |
| 50 | 4.69 | 4.08 | 3.53 | 3.04 | 2.62 |
| 55 | 6.46 | 5.59 | 4.81 | 4.12 | 3.52 |
| 60 | 8.95 | 7.71 | 6.60 | 5.63 | 4.79 |
| 65 | 12.52 | 10.73 | 9.16 | 7.79 | 6.60 |
| 70 | 17.66 | 15.08 | 12.83 | 10.87 | 9.18 |
| 75 | 24.95 | 21.25 | 18.02 | 15.22 | 12.82 |
| 80 | 35.02 | 29.74 | 25.16 | 21.20 | 17.81 |

**Table 8.** Seismic bearing capacity factor $N'_\sigma$ for rock-type sericite with high quartz.

| GSI | $k_h$ = 0 | $k_h$ = 0.05 | $k_h$ = 0.1 | $k_h$ = 0.15 | $k_h$ = 0.2 |
|---|---|---|---|---|---|
| 5 | 0.29 | 0.26 | 0.24 | 0.21 | 0.18 |
| 10 | 0.58 | 0.51 | 0.45 | 0.40 | 0.35 |
| 15 | 1.01 | 0.89 | 0.78 | 0.68 | 0.59 |
| 20 | 1.61 | 1.41 | 1.23 | 1.07 | 0.92 |
| 25 | 2.46 | 2.14 | 1.85 | 1.59 | 1.37 |
| 30 | 3.62 | 3.13 | 2.69 | 2.30 | 1.96 |
| 35 | 5.19 | 4.45 | 3.80 | 3.24 | 2.75 |
| 40 | 7.37 | 6.29 | 5.34 | 4.52 | 3.81 |
| 45 | 10.47 | 8.88 | 7.50 | 6.31 | 5.28 |
| 50 | 14.95 | 12.58 | 10.54 | 8.79 | 7.32 |
| 55 | 21.33 | 17.84 | 14.85 | 12.32 | 10.19 |
| 60 | 30.69 | 25.51 | 21.12 | 17.42 | 14.33 |
| 65 | 44.64 | 36.91 | 30.38 | 24.93 | 20.40 |
| 70 | 65.55 | 53.85 | 44.10 | 35.99 | 29.30 |
| 75 | 96.33 | 78.76 | 64.21 | 52.16 | 42.27 |
| 80 | 140.37 | 114.33 | 92.86 | 75.13 | 60.68 |

In practical engineering, the seismic uniaxial compressive strength bearing capacity coefficients at different seismic intensities are selected and multiplied with the uniaxial compressive strength, $\sigma_c$, of this type of rock to obtain the upper bound of the bearing capacity. For each rock, the parameter $GSI$, which characterizes the mass of the rock mass, is taken to vary in the interval from 5 to 80 in the calculation.

### 5.3. Effect of Horizontal Seismic Coefficient

Figure 15 shows the variation of the upper bound of the bearing capacity for the *intense shear zones* with increases in the horizontal seismic coefficient. The parameters of the rocks in the figure are shown in Table 2, and the surface overload $q_0 = 0$. $\frac{q_u(k_h=0.2)}{q_u(k_h=0)} = 65.3\%$ is taken into consideration. It can be clearly seen that the bearing capacity decreases very severely when $k_h$ increases and is approximately linearly related to the horizontal seismic coefficient. This significant drop indicates that seismic action has a huge weakening effect on the bearing capacity of the foundation, when $k_h$ rises from 0 to 0.2. The predicted value of the ultimate bearing capacity, $q_u$, drops from 10.8 MPa to 7 MPa.

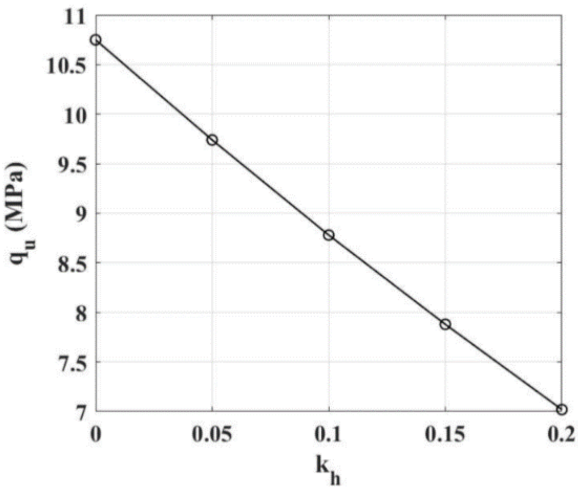


**Figure 15.** Effect of horizontal seismic coefficient, $k_h$, on the upper limit of ultimate bearing capacity, $q_u$.

## 6. Summary and Conclusions

In this research, the effect of seismic action on ultimate bearing capacity of a strip foundation on rock mass was studied using the pseudo-static method. The generalized Prandtl failure mechanism was chosen to simulate the failure critical state of foundations, which is more consistent with the real shape of the soil failure mechanism than the multi-wedge body failure mechanism selected in studies by Yang and Yin [12] and Saada [27]. The modified HB failure criterion was used to calculate the strength of the rock mass. The generalized tangent method proposed by Hoek, based on a wide range of engineering practice [18,19], was adopted to seek the optimal equivalent linear MC criterion envelope of the nonlinear HB envelope. The equivalent envelope was a tangent line to the original nonlinear failure envelope and above the original envelope, to ensure that the calculated value of the bearing capacity was an upper bound value of the bearing capacity. Comparisons were carried out between the results of Yang and Yin [9], obtained by the traditional multi-wedge failure mechanism, and those of the finite element model, which verified the present work. Next, the ultimate bearing capacity of the strip foundation placed on five typical rock masses was calculated by the present method, and the calculated results were compared with the simulation results of the finite element model. Meanwhile, the main deficiency of this study is reflected in the simplification of the seismic forces. This simplification means that the dynamic action of seismic loads was not considered.

Comparing the failure mechanisms of the five rock masses, the following conclusions can be drawn:

1. The calculated value of the equivalent friction angle, $\varphi_t$, is greater for high quality rock, and the ultimate bearing capacity increases as $\varphi_t$ increases.
2. The shapes of the failure mechanisms for different masses are similar when approaching the failure, but with increases in the ultimate bearing capacity, the depth of the mobilized rock mass and the overall volume increase.
3. The angular parameters of the failure mechanism can basically be determined within a general range: the range of values for $\alpha'$ can be set at 55° to 70°, and the better the rock mass, the larger the value taken; $\alpha$ can be set at 87°; and $\delta$ can be set at 90°. The shape of the damage mechanism of the rock foundation can be roughly depicted using this set of parameters.
4. The influence of rock mass bearing capacity parameters $GSI$, $m_i$, and horizontal seismic coefficient, $k_h$, on the upper limit of foundation bearing capacity was evaluated as well. It was found that:
    (1) Decreases in the bearing capacity during an earthquake are significant, and the decrease in bearing capacity will be more drastic with the rise of the surface overload, $q_0$. When the horizontal seismic coefficient, $k_h$, rises from 0 to 0.1, the ultimate bearing capacity, $q_u$, corresponding with the surface overload, $q_0$, of 10 kPa, decreases from 11.4 MPa to 9.3 MPa, with a decrease of 18%. Meanwhile, $q_u$, corresponding with the $q_0$ of 50 kPa, decreases from 13 MPa to 10.4 MPa, with a decrease of 20%.
    (2) The effect of the unit weight, $\gamma$, is lower in contrast to the effect of the surface overload, $q_0$, on the bearing capacity. For the determined overload, $q_0$, as the unit weight, $\gamma$, rises from 20 kN/m$^3$ to 24 kN/m$^3$, the ultimate bearing capacity rises by less than 0.1 MPa, while for the determined unit weight, $\gamma$, the ultimate bearing capacity increases with an increase in surface overload.
    (3) With an increase in $k_h$, the bearing capacity decreases sharply and is approximately linearly related to the horizontal seismic coefficient. This significant drop indicates that seismic action has a huge weakening effect on the bearing capacity of a foundation when $k_h$ rises from 0 to 0.2.
    (4) The bearing capacity coefficient of seismic uniaxial compressive strength, without considering the unit weight of rock mass and surface overload, is also provided in the design tables, which can be used as a reference in practical engineering.

**Author Contributions:** Conceptualization, D.D. and Z.L.; methodology, D.D.; software, Z.L.; validation, D.D. and Z.L.; formal analysis, Z.L.; investigation, D.D.; re-sources, D.D.; data curation, Z.L.; writing—original draft preparation, Z.L.; writing—review and editing, Z.L.; visu-alization, D.D.; supervision, D.D.; project administration, D.D.; funding acquisition, D.D. All authors have read and agreed to the published version of the manuscript.

**Funding:** This research was funded by the Natural Science Foundation of Jiangsu Province grant number BK20210256, the National Natural Science Foundation of China grant number 52108305, the Jiangsu Provincial Dou-ble-Innovation Doctor Program grant number JSSCBS20210068 and the Fundamental Research Funds for the Central Universities.

**Conflicts of Interest:** The authors declare no conflict of interest.

## Notations

| | | | |
|---|---|---|---|
| $q_u$ | bearing capacity of strip footing (MPa) | $q$ | unit vertical load (kPa) |
| $c$ | cohesion values of soil (kPa) | $F_h$ | horizontal force caused by earthquakes (kN/m) |
| $q_0'$ | equivalent uniform load (kPa) | $k_h$ | average horizontal seismic coefficient |
| $\gamma$ | unit weight of soil or rock mass (kN/m3) | $\sigma_1, \sigma_3$ | major and minor principal stresses (MPa) |
| $B_0$ | width of strip foundation (m) | $\tau$ | shear stress (kPa) |
| $N_c$, $N_q$, $N_\gamma$ | the coefficients of Terzaghi bearing capacity | $\alpha, \alpha', \delta$ | angular parameters describing the shape of Generalized Prandtl failure mechanism (°) |
| $m$ | material constants describing the type of rock mass | $v_0, v_1, v_p, v_{p0}$ | velocity of the parts of Generalized Prandtl failure mechanism (m/s) |
| $s$ | material constants describing the integrity of rock mass | $W_e, W_{e1}, W_{e2}, \ldots$ | work done by the external forces (J) |
| $GSI$ | geological strength index characterizing the quality of rock mass | $f_1, f_2, f_3$ | functions reflecting the influence of the unit weight of rock mass |
| $n$ | material constants depending on $GSI$ | $f_4$ | function reflecting the influence of surface overload |
| $\varphi$ | friction angle of soil (°) | $f_1', f_2', f_3', f_4'$ | functions reflecting the influence of the horizontal seismic acceleration |
| $m_i$ | $m$-value of the intact rock mass | $W_i, W_{i1}, W_{i2}, \ldots$ | internal energy dissipation rate of the failure mechanism (J) |
| $c_t$, $\varphi_t$ | equivalent cohesion and tangent angle of rock mass (kPa, °) | $g_1, g_2, g_3, g_4$ | function reflecting the influence of internal energy dissipation |
| $\sigma_c$ | uniaxial compressive strength of rock(MPa) | $\theta, \alpha_i, \beta_i, k$ | parameters describing the shape of Multi-wedge failure mechanism |
| $e_1, e_2$ | principal axes of the right-angle coordinate $e_1$system in Figure 1. being the horizontal axis and $e_2$ the vertical axis | $\sigma_{3n}, \sigma_{3max}, \sigma_{cm}$ | parameters describing the strength of a rock mass (MPa) |
| $D$ | depth of embedment of the foundation(m) | $H$ | the depth of layer, which is assumed to be 100 m in this study (m) |
| $Q$ | vertical load from the superstructure (kN/m) | $N_\sigma'$ | seismic uniaxial compressive strength bearing capacity coefficient |
| $q_0$ | surface overload on the ground (kN) | | |

## References


1. Ausilio, E.; Conte, E.; Dente, G. Seismic stability analysis of reinforced slopes. *Soil Dyn.* **2000**, *19*, 159–172. [CrossRef]
2. Meyerhof, G.G. The ultimate bearing capacity of foundations. *Géotechnique* **1951**, *2*, 301–332. [CrossRef]
3. Zhu, D.Y.; Lee, C.F.; Jiang, H.D. A numerical study of the bearing capacity factor $N\gamma$. *Can. Geotech. J.* **2001**, *38*, 1090–1096. [CrossRef]
4. Gao, Y.F.; Zhang, F.; Lei, G.H.; Li, D.Y. An extended limit analysis of three-dimensional slope stability. *Géotechnique* **2013**, *63*, 518–524. [CrossRef]
5. Yuan, W.; Li, J.X.; Li, Z.H.; Wang, W.; Sun, X.Y. A strength reduction method based on the Generalized Hoek-Brown (GHB) criterion for rock slope stability analysis. *Comput. Geotech.* **2020**, *117*, 103240.
6. Saada, Z.; Maghous, S.; Garnier, D. Bearing capacity of shallow foundations on rocks obeying a modified Hoek-Brown failure criterion. *Comput. Geotech.* **2008**, *35*, 144–154. [CrossRef]
7. Li, Y.X.; Yang, X.L. Three-dimensional seismic displacement analysis of rock slopes based on Hoek-Brown failure criterion. *KSCE J. Civ. Eng.* **2018**, *22*, 4334–4344. [CrossRef]
8. Du, D.C.; Dias, D.; Do, N. A Simplified Way to Evaluate the Effect of Temperature on a Circular Tunnel. *Geotechnics* **2021**, *1*, 385–401. [CrossRef]
9. Michalowski, R.L. Limit loads on reinforced foundation soils. *J. Geotech. Geoenviron.* **2004**, *130*, 381–390. [CrossRef]
10. Du, D.C.; Dias, D.; Do, N. Effect of surcharge loading on horseshoe-shaped tunnels excavated in saturated soft rocks. *JRMGE* **2020**, *12*, 1339–1346. [CrossRef]
11. Du, D.C.; Dias, D.; Do, N. U-shaped tunnel lining design using the Hyperstatic Reaction Method—Influence of the invert. *Soils Found.* **2020**, *60*, 592–607. [CrossRef]
12. Yang, X.L.; Yin, J.H. Upper bound solution for ultimate bearing capacity with a modified Hoek-Brown failure criterion. *Int. J. Rock. Mech. Min.* **2005**, *42*, 550–560. [CrossRef]
13. Tang, J.; Liu, Y.B. Bearing capacity calculation of rock foundation based on nonlinear failure criterion. *IERI Proc.* **2012**, *1*, 110–116.
14. Al-Bittar, T.; Abdul-Hamid, S. Bearing capacity of spatially random rock masses obeying Hoek-Brown failure criterion. *Georisk Assess. Manag. Risk Eng. Syst. Geohazards* **2016**, *11*, 215–229. [CrossRef]

15. Yu, H.S.; Salgado, R.; Sloan, S.W.; Kim, J.M. Limit analysis versus limit equilibrium for slope stability. *J. Geotech. Geoenviron.* **1998**, *124*, 1–11. [CrossRef]
16. Kim, J.M.; Salgado, R.; Lee, J. Stability analysis of complex soil slopes using limit analysis. *J. Geotech. Geoenviron.* **2002**, *128*, 546–557. [CrossRef]
17. Hoek, E. Estimating Mohr-Coulomb friction and cohesion values from the Hoek-Brown failure criterion. *Int. J. Rock Mech. Min.* **1990**, *27*, 227–229. [CrossRef]
18. Hoek, E.; Brown, E.T. The Hoek-Brown failure criterion and GSI-2018 edition. *JRMGE* **2019**, *11*, 445–463. [CrossRef]
19. Hoek, E.; Carranza, T.C.; Corkum, B. Hoek-Brown failure criterion-2002 edition. *Proc. Fifth N. Am. Rock Mech. Symp.* **2002**, *1*, 267–273.
20. Zhu, H.H.; Zhang, Q.; Zhang, L.Y. Review of research progresses and applications of Hoek-Brown strength criterion. *Rock Mech. Rock Eng.* **2013**, *32*, 1945–1963.
21. Zhu, H.H.; Zhang, Q. A constitutive model based on the modified generalized three-dimensional Hoek–Brown strength criterion. *Int. J. Rock Mech. Min. Sci.* **2017**, *98*, 78–87. [CrossRef]
22. Zhu, H.H.; Zhang, Q.; Zhang, L.Y. Modification of a generalized three-dimensional Hoek–Brown strength criterion. *Int. J. Rock Mech. Min. Sci.* **2013**, *59*, 80–96.
23. Hasanzadehshooiili, H.; Lakirouhani, A.; Medzvieckas, J. Evaluating elastic-plastic behaviour of rock materials using Hoek-Brown failure criterion. *J. Civ. Eng. Manag.* **2012**, *18*, 402–407. [CrossRef]
24. Chen, W.F. *Limit Analysis and Soil Plasticity*; Elsevier: Amsterdam, The Netherlands, 1975.
25. Drescher, A.; Christopoulos, C. Limit analysis slope stability with nonlinear yield condition. *Int. J. Numer. Anal. Met.* **1988**, *12*, 341–345. [CrossRef]
26. Collins, I.F.; Gunn, C.I.M.; Pender, M.J.; Wang, Y. Slope stability analyses for materials with a non-linear failure envelope. *Int. J. Numer. Anal. Met.* **1988**, *12*, 12533–12550. [CrossRef]
27. Saada, Z.; Maghous, S.; Garnier, D. Seismic bearing capacity of shallow foundations near rock slopes using the generalized Hoek-Brown criterion. *Int. J. Numer. Anal. Met.* **2011**, *35*, 724–748. [CrossRef]
28. Mao, J.Z.; Huang, Z.W.; Xiao, L.P.; Du, S.H. Prediction of mechanical parameters of the surrounding rock based on Hoek-Brown criterion. *IOP Conf. Ser. Earth Environ. Sci.* **2020**, *570*, 052071. [CrossRef]